Journal of Power Sources 191 (2009) 269–274

Contents lists available at ScienceDirect

Journal of Power Sources

journal homepage: www.elsevier.com/locate/jpowsour

Phase stability of $Sm_{0.5}Sr_{0.5}CoO_3$ cathodes for on-planar type, single-chamber, solid oxide fuel cells

Hwa Seob Song[a], Ji-Hyun Min[a], Joosun Kim[b], Jooho Moon[a,*]

[a] Department of Materials Science and Engineering, Yonsei University, Seoul 120-749, Republic of Korea
[b] Center for Energy Materials Research, Korea Institute of Science and Technology, Seoul 136-791, Republic of Korea

ARTICLE INFO

Article history:
Received 26 December 2008
Received in revised form 21 January 2009
Accepted 3 February 2009
Available online 20 February 2009

Keywords:
$Sm_{0.5}Sr_{0.5}CoO_3$
Decomposition
Reduction mechanism
Perovskite cathode
Solid oxide fuel cell

ABSTRACT

The stability of $Sm_{0.5}Sr_{0.5}CoO_3$ (SSC) under reduction conditions is investigated to determine whether it can be used as a cathode material in on-planar type, single-chamber, solid oxide fuel cells. The techniques of X-ray diffraction, X-ray photoelectron spectroscopy and scanning electron microscopy are used to reveal the reduction mechanism of SSC. Impedance spectroscopy analysis also provides a better understanding of the influence of decomposed SSC phases on cathode performance. Decomposition of SSC occurs on the surface by the formation of dot-shaped SrO, $Co(OH)_2$ and CoO on top of the reduced SSC layer at 250 °C in 4% H_2O–96% H_2. The SSC perovskite structure is destroyed at 350 °C in pure hydrogen. There is a catastrophic microstructural change in which SSC is completely decomposed to SrO and CoO that cover the surface of Sm_2O_3.

1. Introduction

Single-chamber solid oxide fuel cells (SC-SOFCs) consist of only one gas chamber where both the anode and the cathode are exposed to the same mixture of fuel and air. This unique configuration gives SC-SOFCs various advantages over conventional SOFCs. First, the gas sealing problem can be inherently avoided since no separation between fuel and air is required. Second, hydrocarbon fuels are directly utilized without carbon deposition due to the presence of a large amount of oxygen in the gas mixture. The simplified cell structure associated with SC-SOFCs endows mechanical and thermal stabilities and the operation temperature is self-sustained due to the exothermic partial oxidation of the fuel [1–5]. In this regard, SC-SOFCs are suitable for various applications, such as distributed power generators and portable power sources. Recent research has focused on the development of low-temperature SC-SOFCs by the adaptation of novel materials [6,7].

Reducing the operating temperature requires the use of electrolytes with high ionic conductivity and cathodes with low polarization resistance. Rare earth-doped cobaltite like $Sm_{0.5}Sr_{0.5}CoO_3$ (SSC) has attracted much attention as a cathode because of its high mixed ionic and electronic conductivities at lower temperatures [8]. Sm doped ceria (SDC) is a good candidate for a low-temperature electrolyte and does not form undesirable secondary phases when in contact with the SSC cathode during operation. These materials are selected to fabricate low-temperature, on-planar type SC-SOFCs in which both the anode and cathode are located on the same side of the electrolyte. The ohmic resistance can be reduced by decreasing the gap between the anode and the cathode instead of using a thin electrolyte film. Such a cell configuration works well with miniaturization and integration for micro-/mini-SOFC applications. On the other hand, the electrolyte surface between the electrodes meets the reducing gas during the anode reduction step prior to measurement so that he exposed SDC electrolyte may undergo reduction, thereby losing its ionic conductivity.

In our previous research, we suggested [9] 250 °C, 4% H_2O–96% H_2 as the optimum reduction conditions for the anode (Ni-SDC) on top of an SDC electrolyte-based SC-SOFC. Only NiO is reduced to Ni while suppressing electronic conduction in the SDC electrolyte. In that work, however, only the anode was considered when selecting these specific conditions. The reduction conditions should also be carefully controlled so as to not damage the cathode. In fact, it has been reported [10–12] that SSC is unstable at very low partial pressures of oxygen. In this study, we have investigated the stability of SSC in Ni-SDC (anode)/SDC (electrolyte)/SSC (cathode) on-planar type SC-SOFCs. The electrical properties, phase composition and structural variation of SSC are studied to understand the phase stability and decomposition behaviour of SSC.

* Corresponding author. Tel.: +82 2 2123 2855; fax: +82 2 365 5882.
E-mail address: jmoon@yonsei.ac.kr (J. Moon).

0378-7753/$ – see front matter © 2009 Elsevier B.V. All rights reserved.
doi:10.1016/j.jpowsour.2009.02.028

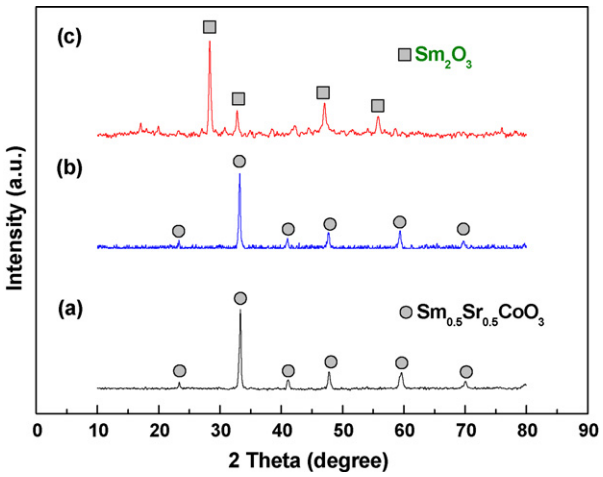

Fig. 1. XRD patterns for SSC: (a) as-sintered; (b) after reduction at 250 °C in 4% H_2O–96% H_2; (c) after reduction at 350 °C in pure H_2.

2. Experimental

Commercially available SSC (Seimi Chemical Co., Japan) powders were mixed with polyvinylpyrrolidone (PVP, Aldrich Chem., USA) and di-*n*-butyl phthalate (DBP, Yakuri Pure Chem. Co., Japan) as a binder and a plasticizer, respectively. The powder mixture was uni-axially pressed under hydraulic pressure (70 MPa), followed by sintering at 1000 °C in air for 4 h. Then, the sintered SSC discs were reduced at either 250 °C in 4% H_2O–96% H_2 (denoted *condition I*) or 350 °C in pure H_2 (denoted *condition II*) for 24 h. Microstructural and phase analyses of the SSC before and after each reduction were conducted by means of scanning electron microscopy (SEM, JSM-6500F, JEOL). Bulk phase and surface compositions were analyzed by X-ray diffraction (XRD, Rigaku D-max) and X-ray photoelectron spectroscopy (XPS, SIGMA PROBE ThermoVG), respectively. The degradation in the cathodic performance of SSC before and after reduction was indirectly determined by measuring the d.c. conductivity and polarization resistance. The electrical conductivity of a sintered bar-shaped SSC sample (5 mm × 3 mm × 20 mm) was monitored by the 4-point probe method over during a 12 h exposure to the reduction atmosphere of 4% H_2O–96% H_2 at 250 °C.

A SSC/SDC/SSC symmetric half-cell was prepared by the screen printing method with the paste materials comprised of a mixture of the SSC powders and additives dispersed in an organic solvent. The cathode layer was placed on both sides of a 0.5 mm thick SDC disc for the measurement of interfacial polarization resistance. Platinum mesh connected to a platinum lead wire was attached to the cathode layers with platinum paste for current-collection. The area of the applied SSC cathode was 1.5 cm^2 and the thickness was 15–20 μm. The cathode and current-collection layer were sintered at 1000 °C for 4 h and at 850 °C for 30 min. Electrochemical impedance measurements were performed under three different oxygen partial pressures (0.2, 0.1, and 0.01 atm) before and after reduction under *condition I* using a Solartron SI 1260/1287. The impedance spectra were obtained at 700 °C over a frequency range of 100 kHz to 1 mHz with an applied a.c. voltage amplitude of 20 mV.

3. Results and discussion

The phase stability of the sintered SSC before and after exposure to the reduction atmospheres of *condition I* and *condition II* is shown in Fig. 1. The XRD diffraction patterns of the as-sintered SSC match well with those of the phase-pure perovskite $Sm_{0.5}Sr_{0.5}CoO_3$, as shown in Fig. 1a [13]. There is no noticeable difference in the diffraction peaks between the as-sintered SSC and the SSC reduced

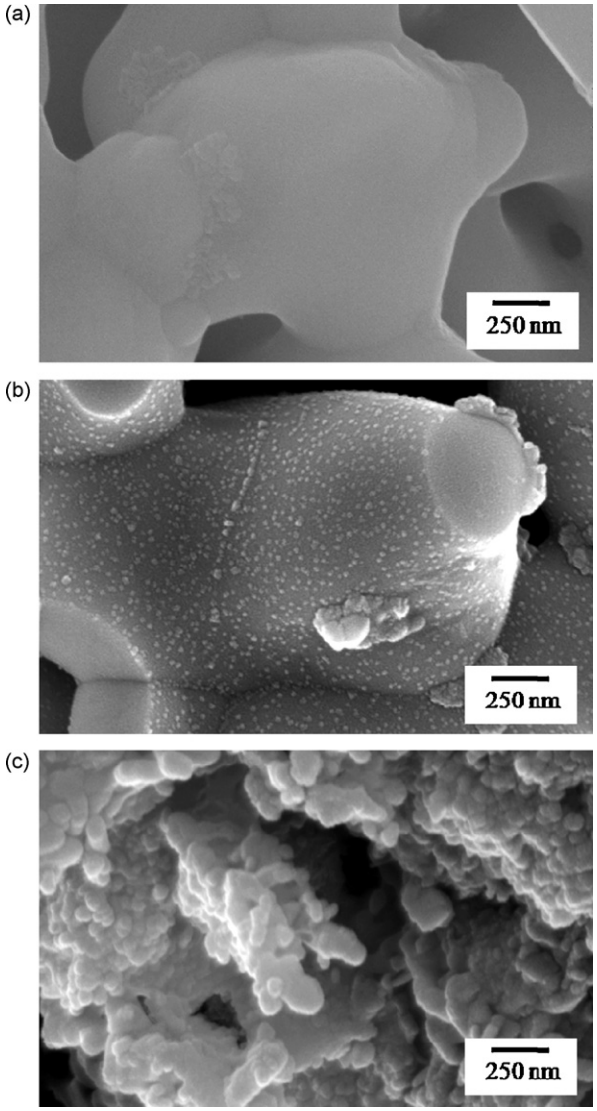

Fig. 2. Cross-sectional SEM images of SSC: (a) as-sintered; (b) after reduction at 250 °C in 4% H_2O–96% H_2; (c) after reduction at 350 °C in pure H_2.

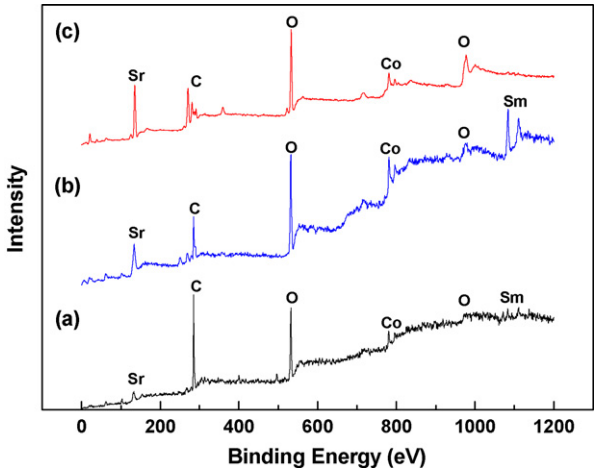

Fig. 3. XPS wide-scan results of SSC: (a) as-sintered; (b) after reduction at 250 °C in 4% H_2O–96% H_2; (c) after reduction at 350 °C in pure H_2.

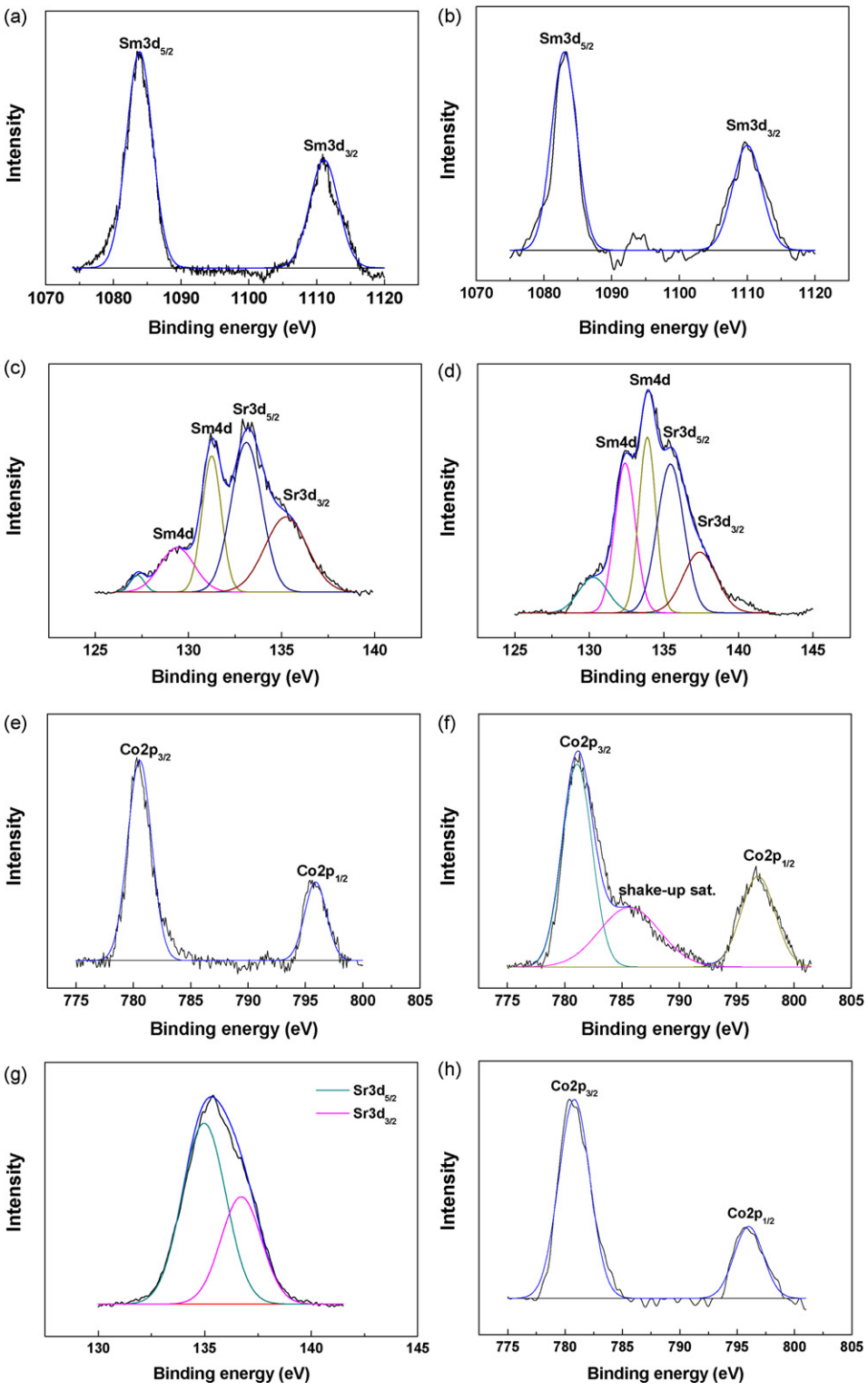

Fig. 4. XPS narrow scan results showing elements comprising SSC: Sm spectra (a) as-sintered and (b) reduced under *condition I*; Sr spectra (c) as-sintered and (d) reduced under *condition I*; Co spectra (e) as-sintered and (f) reduced under *condition I*; Sr spectra (g) as-sintered and (h) reduced under *condition II*.

under *condition I* (Fig. 1b). By contrast, the SSC phase disappears after exposure to reduction *condition II* and only the Sm_2O_3 (JCPDS, 25-0749) phase is detected (Fig. 1c). This indicates that SSC undergoes significant decomposition at 350 °C under a highly reducing atmosphere.

The microstructure of the sintered SSC as a function of the reduction atmosphere was investigated by SEM. Fig. 2a shows a cross-sectional view of the as-sintered SSC at 1000 °C in which an interconnected granular structure with smooth surfaces is observed. Reduction under *condition I* causes a change in microstructure (Fig. 2b), but XRD analysis does not detect any phase change. The surface becomes rough due to the formation of many ~20 nm-sized protrusions that give rise to raspberry-like surface structure. The change in microstructure is dramatically intensified

upon exposure to reduction *condition II*, as shown in Fig. 2c. The porous granular framework collapses into aggregated particles of about 100–200 nm in size and the reduced sintered SSC sample becomes fragile. Based on these microstructural observations, it is reasonable to assume that SSC undergoes complete decomposition when exposed to the reducing atmosphere.

To gain an in-depth understanding of the SSC phase decomposition, XPS was used to analyze the surface composition of the sintered SSC. Wide-scan spectra for the three different samples are presented in Fig. 3. All of the metallic components, i.e., Sm, Sr and Co atoms, are detected for both the as-sintered SSC and the SSC exposed to reduction *condition I*, as witnessed in Fig. 3a and b. By contrast, the sample exposed to reduction *condition II* shows only Sr and Co atoms. This implies that the crystalline Sm_2O_3 detected by XRD is in the interior, whereas the surface is covered by substances containing only Sr and Co atoms. These phases might be crystalline if the amount present is sufficiently below the XRD detection limit.

Narrow-scan XPS data for both sintered SSC and SSC reduced under *conditions I* and *II* are given in Fig. 4. In general, the shift in the binding energy (BE) of a core level is correlated with the change in chemical potential, the variation in the number of valence electrons on the atom considered, or the shift in the extra-atomic relaxation energy [14]. This means that a change in binding energy can reflect the surface reduction process of the cathode. The binding energy of Sm $3d_{5/2}$ is 1083.3 eV for the sintered SSC (Fig. 4a) and 1083.9 eV for the reduced SSC (Fig. 4b). Thus, it is not possible to distinguish between $Sm_{0.5}Sr_{0.5}CoO_3$ and Sm_2O_3 based on the BE of Sm $3d_{5/2}$ since they are almost identical [15].

The Sr peaks interfere with the Sm peak and can be deconvoluted into five sub-peaks originating from both Sm 4d and Sr $3d_{5/2}$. This means that the phases containing Sm or Sr atoms co-exist on the cathode surface. The BE of Sr $3d_{5/2}$ is 133.1 eV for the sintered SSC (Fig. 4c), which matches with the BE of Sr in $La_{1-x}Sr_xMnO_3$ perovskite and thereby indicates the presence of SSC [14]. The BE shifts 2.3 eV higher (135.4 eV) for the reduced SSC (Fig. 4d), which is identical to the BE of Sr in SrO [15], and implies that the SSC surfaces are partially reduced under *condition I* to form SrO on the surfaces. The sintered SSC displays Co 2p spin–orbit splitting at 780.2 and 796 eV, corresponding to the Co $2p_{3/2}$ and Co $2p_{1/2}$ levels, respectively, which are indicative of the presence of Co^{3+} ions (Fig. 4e). For the reduced SSC, the BE shifts to a higher level (781.1 eV) identical to the BEs of Co in $Co(OH)_2$ (Fig. 4f) [15]. Moreover, the shake-up satellite peak at 785.7 eV implies the presence of Co^{2+} [16,17] in the form of CoO. The XPS spectra reveal that the SSC surface completely decomposes into SrO and CoO covering the entire surface when reduced under *condition II* (Fig. 4g and h). The binding energies of Sr $3d_{5/2}$ and Co $2p_{3/2}$ are 135.2 and 780.4 eV, respectively, which exactly match the binding energies of Sr^{2+} for SrO and Co^{2+} for CoO. The CoO phase probably originates from full re-oxidation of the decomposed $Co(OH)_2$. The XPS results, together with SEM images, support the fact that the SSC surface structure collapses into SrO and CoO which block the detection of the underlying crystalline Sm_2O_3 phase.

Electrical conductivity was measured to verify the surface reduction of SSC. The variation in conductivity of the SSC bar sample when reduced under *condition I* is presented in Fig. 5. The initial conductivity is 2300 S^{-1} cm, but decreases with time to about 73 S^{-1} cm after 8 h. SSC is a p-type semiconductor in which the hole is transported by a hopping mechanism and aliovalent doping of Sr allows an increase in hole concentration. In fact, the electrical conductivity of $Sm_{1-x}Sr_xCoO_3$ depends markedly on the Sr content. At 250 °C, $Sm_{1-x}Sr_xCoO_3$ has a conductivity of over 1500 S^{-1} cm when $x = 0.5$, but it falls below 1 S^{-1} cm when $x = 0$ [18]. In the present reduction experiment, SSC loses its electrical conductivity due to a decreased hole concentration as the surface SrO forms out of the perovskite structure. If the electrical conductivity of the decomposed surface

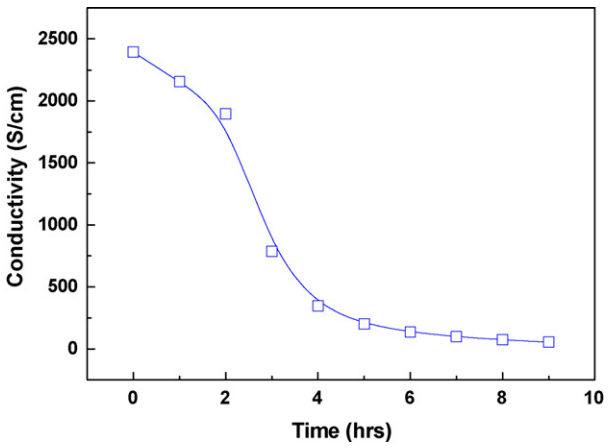

Fig. 5. Conductivity variation of SSC bar sample on exposure to a 4% H_2O–96% H_2 atmosphere at 250 °C.

phases is 1000 times less than that of $Sm_{0.5}Sr_{0.5}CoO_3$, i.e., like $SmCoO_3$, it can be estimated that the volume (2 vol.%) of decomposed SSC accounts for 98% of the reduction in conductivity using a mixture rule. The XRD technique is suitable for identifying the major constituent phases, but it often fails to detect the presence of substances at less than 5 vol.% [19]. The degradation in electrical conductivity indicates the formation of less conductive and/or insulating phases such as SrO-deficient $SmCoO_3$, CoO, $Co(OH)_2$, and SrO on the surface.

The proposed mechanism of SSC decomposition under reduction conditions is illustrated in Fig. 6. $Sm_{0.5}Sr_{0.5}CoO_3$ is partially decomposed into dot-shaped SrO, $Co(OH)_2$ and CoO, as expressed by Eq. (1), leaving behind $Sm_{0.5}Sr_{0.5-x}Co_{1-y-z}O_{3-x-y-z}$ under reduction *condition I* (Fig. 6a). It is believed that $Sm_{0.5}Sr_{0.5-x}Co_{1-y-z}O_{3-x-y-z}$ retains the perovskite structure so as

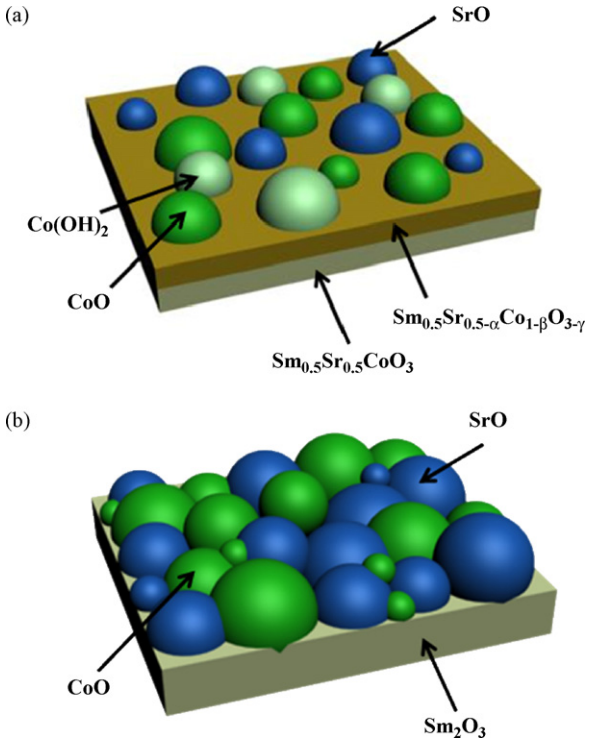

Fig. 6. Proposed decomposition mechanism of SSC at reduction conditions of (a) 250 °C in 4% H_2O–96% H_2 and (b) 350 °C in pure H_2.

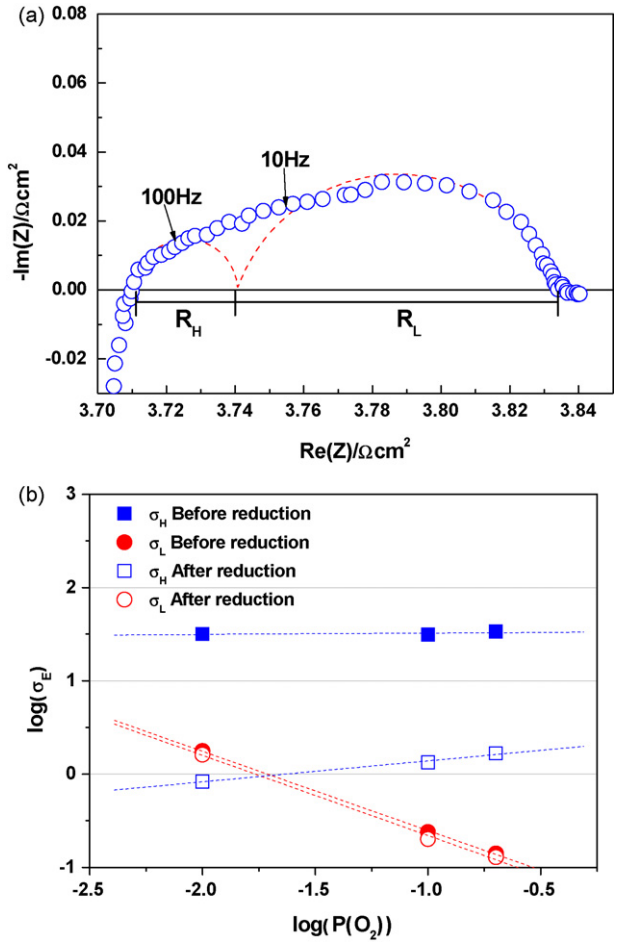

Fig. 7. (a) Cole–cole plot obtained for cathode ($P_{O_2} = 0.21$ atm) and (b) interfacial conductivities as function of oxygen partial pressure. Conductivity calculated is based on resolved interfacial resistance obtained in part (a).

to maintain a coherent interface with the inner $Sm_{0.5}Sr_{0.5}CoO_3$.

$$Sm_{0.5}Sr_{0.5}CoO_3 + yH_2O \rightarrow Sm_{0.5}Sr_{0.5-x}Co_{1-y-z}O_{3-x-y-z} + xSrO + yCo(OH)_2 + zCoO \quad (1)$$

The SSC reduction is accelerated and the material is completely decomposed into SrO and CoO on top of Sm_2O_3 under reaction *condition II* (Fig. 6b). This reaction is represented by:

$$2Sm_{0.5}Sr_{0.5}CoO_3 \rightarrow \tfrac{1}{2}Sm_2O_3 + SrO + 2CoO + \tfrac{3}{4}O_2 \quad (2)$$

Electrochemical impedance measurements were also performed as a function of the oxygen partial pressure (P_{O_2}) for both the as-sintered SSC and the SSC reduced under *condition I*. Fig. 7a shows a cole–cole plot of the SSC cathode half-cell measured at 700 °C. The impedance spectra are separated into a low-frequency resistance (R_L) and a high-frequency resistance (R_H) using an equivalent circuit model. Each resolved resistance corresponds to a particular electrode reaction. The interfacial conductivity (σ) can be derived from the interfacial polarization resistance (R) using the Eq. (3) where A is the electrode area [20]:

$$\sigma = \frac{1}{AR} \quad (3)$$

The calculated interfacial conductivity obtained from the impedance results is presented in Fig. 7b as a function of the oxygen partial pressure. The low-frequency interfacial conductivities (σ_L) remain virtually unchanged during the reduction process, whereas the high-frequency interfacial conductivities (σ_H) decrease after reduction regardless of sample type. This also shows that σ_H is nearly independent of the oxygen partial pressure, while it is known that the magnitude of σ_H reflects the ease of oxygen species transport [21]. The formation of non-ionic conducting phases such as SrO, $Co(OH)_2$ and CoO adversely affect the transport of oxide ions or oxygen intermediates. By contrast, σ_L shows a dependency on oxygen partial pressure, but remains constant before and after reduction under *condition I*. It has been reported that the polarization resistance at lower frequencies is related to the gas diffusion ability through the electrode [20]. The invariance of σ_L before and after the reduction suggests that reduction under *condition I* does not bring about a microstructural change, as seen in SEM images (Fig. 2). This observation indicates that SSC cathodic performance degrades because the SSC surface decomposition induces a lowering of ionic conductivity.

4. Conclusions

It has been found that SSC cathodes used in on-planar type SC-SOFC become unstable in reduction atmospheres. The SSC cathodes can be decomposed by exposure to reducing atmospheres during the anode reduction process. Under reduction *condition I* (250 °C, 4% H_2O–96% H_2), perovskite SSC transforms to SrO, $Co(OH)_2$ and CoO on the surface of the reduced SSC, i.e., the $Sm_{0.5}Sr_{0.5-\alpha}Co_{1-\beta}O_{3-\gamma}$ layer. Under reduction *condition II* (350 °C, H_2), SSC completely decomposes into Sm_2O_3, SrO and CoO phases as the perovskite structure is destroyed and there is an abrupt change in microstructure. The SSC decomposition is confirmed by monitoring the variation in both electrical conductivity and interfacial polarization resistance. The SSC loses its electrical conductivity and the cathodic resistance increases on exposure to the reduction atmosphere. This indicates that the performance of a SSC cathode degrades due to the formation of less electronic and ionic conducting phases on the surface. In this regard, SSC cannot be used in on-planar type SC-SOFCs and other cathode materials with better reduction stability should be employed.

Acknowledgements

This work was supported by a Korean Research Foundation Grant (KRF-2007-313-D00338). It was also partially supported by the Korea Science and Engineering Foundation (KOSEF) through the National Research Laboratory Program funded by the Ministry of Education, Science and Technology (No. R0A-2005-000-10011-0).

References

[1] T. Hibino, H. Tsunekawa, S. Tanimoto, M. Sano, J. Electrochem. Soc. 147 (4) (2000) 1338–1343.
[2] T. Hibino, A. Hashimoto, T. Inoue, J. Tokuno, S. Yoshida, M. Sano, Science 288 (2000) 2031–2033.
[3] Z. Shao, S.M. Haile, Nature 431 (2004) 170–173.
[4] T. Suzuki, P. Jasinski, V. Petrovsky, H.U. Anderson, F. Dogan, J. Electrochem. Soc. 151 (2004) A1473–A1476.
[5] T. Suzuki, P. Jasinski, H.U. Anderson, F. Dogan, J. Electrochem. Soc. 151 (2004) A1678–A1682.
[6] B.C.H. Steele, A. Heinzel, Nature 414 (2001) 345–352.
[7] B.C.H. Steele, Solid State Ionics 134 (2000) 3–20.
[8] T. Ishihara, M. Honda, T. Shibayama, H. Minami, H. Nishiguchi, Y. Takita, J. Electrochem. Soc. 145 (1998) 3177–3183.
[9] J.H. Min, S.J. Ahn, J. Moon, J. Kim, J. Kor. Ceram. Soc. 44 (2007) 542–547 (in Korean).
[10] B.A. Boukamp, Nature Mater. 2 (2003) 294–296.
[11] A. Sin, E. Kopnin, Y. Dubitsky, A. Zaopo, A.S. Arico, L.R. Gullo, D. La Rosa, V. Antonucci, J. Power Sources 145 (2005) 68–73.
[12] S. Piñol, J. Fuel Cell Sci. Technol. 3 (2006) 434–437.
[13] Z. Haizhou, C. You, Y. Weishen, Chin. J. Catal. 29 (1) (2008) 7–9.
[14] J. Matsuno, A. Fujimori, Y. Takeda, M. Takano, Europhys. Lett. 59 (2) (2002) 252–257.

[15] John F. Moulder, William F. Stickle, Peter E. Sobol, Kenneth D. Bomben, in: J. Chastain (Ed.), Handbook of X-ray Photoelectron Spectroscopy, Perkin-Elmer Corporation Physical Electronics Division, Minnesota, 1992, pp. 148–149.
[16] R. Lago, G. Bini, M.A. Peña, J.L.G. Fierro, J. Catal. 167 (1997) 198–209.
[17] M. Crespin, W.K. Hall, J. Catal. 69 (1981) 359.
[18] H.Y. Yu, Y. Takeda, N. Imanishi, O. Tamamoto, Solid State Ionics 100 (1997) 283–288.
[19] T.A. Brettell, K. Inman, N. Rudin, R. Saferstein, Anal. Chem. 73 (2001) 2735–2744.
[20] M. Koyama, C. Wen, T. Masuyama, J. Otomo, H. Fukunaga, K. Yamada, K. Eguchi, H. Takahashi, J. Electrochem. Soc. 148 (2001) A795–801.
[21] H.S. Song, S.H. Hyun, J. Kim, H.-W. Lee, J. Moon, J. Mater. Chem. 18 (2008) 1087–1092.